

MODELING OF FAST REACTOR CLADDING FAILURE FOR HYPOTHETICAL ACCIDENT TRANSIENT ANALYSIS

J. M. KRAMER, R. J. DIMELFI, T. H. HUGHES, L. W. DEITRICH

*Reactor Analysis and Safety Division, Argonne National Laboratory,
9700 South Cass Avenue, Argonne, Illinois 60439, U.S.A.*

D 7/2

Summary

An analysis is made of burst experiments performed on neutron irradiated cladding tubes. This is done by employing a generalized Voce equation to describe the mechanical deformation of type 316 stainless steel, combined with an empirical creep crack growth law, each modified to account for the effects of irradiation matrix hardening, and irradiation induced grain boundary embrittlement, respectively.

The results of this analysis indicate that for large initial hoop stress, failure occurs at relatively low temperature and is controlled by the onset of plastic instability. The increase in failure temperature of irradiated material, in this low temperature region, is due to irradiation strengthening. Failure in the case of relatively small initial hoop stress occurs at high temperature where the Voce equation reduces to a power law creep formula. The ductility of irradiated material, in this high temperature region, is adequately described through the use of an empirical intergranular crack growth law used in conjunction with the creep law. The effect of neutron irradiation is to reduce the activation energy for crack propagation from the value for creep to some lower value correlated to independent Dorn rupture parameter measurements. The result is a predicted reduced ductility which translates into a reduction in failure temperature at a given hoop stress value for irradiated material.

1. Introduction

The response of fast breeder reactor fuel to accident transients is often such that substantial loads are imposed upon the fuel cladding. The cladding can simultaneously be subjected to rapid temperature increases which accompany the accident sequence. Consequently, cladding failure can occur over a wide range of temperature and ductility, depending on the intensity of the resulting applied stress and the nature of the predominant rupture mode. Understanding the character of the cladding breach is important, since the time, location and extent of failure can influence aspects of fuel motion which, in turn, can affect the ultimate course of the accident.

In order to understand better the mechanical response and failure behavior of liquid metal fast breeder reactor cladding material, a number of experiments, aimed at simulating certain accident conditions have been performed [1]. In these tests, pressurized tubes of 20% cold-worked type 316 stainless steel are uniformly heated at a constant rate until failure occurs. The ductility and temperature at failure are reported. These experiments have been performed on both unirradiated material, and on cladding tubes irradiated to various neutron fluence levels. In an earlier work [2], the authors have analyzed the failure behavior of the unirradiated material, dividing rupture into high and low temperature regimes. An analysis of tube burst experiments performed on the irradiated material is the subject of the present paper. To treat the failure of irradiated tubes, the salient features of the authors' earlier work are maintained, but modified in basically two ways. A treatment of irradiation hardening is included in the low temperature rupture analysis, and the concept of grain boundary embrittlement is included in the high temperature rupture analysis.

2. Constitutive Equations

2.1 Basic Equations

Pressurization of the cladding tubes results essentially in a 2:1 biaxial stress state from which and an equivalent stress $\bar{\sigma}$ and an equivalent plastic strain $\bar{\epsilon}_p$ may be defined. The relationship between these two quantities, including the temperature and strain rate dependence, can be extracted from a generalized Voce equation in which the flow stress $\bar{\sigma}$ for annealed material is given by

$$\bar{\sigma} = \sigma_s - \left[\sigma_s - \sigma_1 \right] \exp \left(- \frac{\hat{\epsilon}}{\epsilon_c} \right) . \quad (1)$$

Here $\hat{\epsilon}$ is a hardness parameter which, in this paper, includes the effects of strain hardening and irradiation hardening, and satisfies the relationship

$$\frac{d\hat{\epsilon}}{dt} = \left| \frac{d\bar{\epsilon}_p}{dt} \right| + \frac{d\epsilon_c}{dt} \quad (2)$$

where $\frac{d\bar{\epsilon}_p}{dt}$ is the plastic strain rate and $\frac{d\epsilon_c}{dt}$ is the irradiation hardening rate. In Eq. (1), σ_1 is the yield stress of fully annealed unirradiated material; and σ_s is the saturation value approached by the flow stress as $\hat{\epsilon}$ increases. Also, σ_s , σ_1 and ϵ_c are temperature and strain-rate-dependent material functions chosen so that at low temperature and high strain rate they are only temperature dependent, but at high temperature and low strain rate Eq. (1) reduces to the familiar power law creep equation

$$\bar{\sigma}^n = \frac{1}{C_0} \frac{d\bar{\epsilon}_p}{dt} \exp \left(\frac{Q_c}{RT} \right) . \quad (3)$$

Here, Q_c is the activation energy for creep, R is the gas constant, T is the absolute temperature, and C_o is only a weak function of temperature which will be assumed constant.

In the high temperature creep deformation regime, ductility is often limited by intergranular fracture. This situation becomes even more severe for irradiated material due to induced grain boundary embrittlement. For this reason, a relation describing grain boundary crack growth must be included among the system of equations under consideration. An empirical crack growth law having the form

$$\frac{d\ell}{dt} = B_o K_I^m \exp\left(-\frac{Q_\ell}{RT}\right) \quad (4)$$

has been chosen. In Eq. (4), ℓ is the crack length, K_I is the linear elastic (mode I) stress intensity factor, Q_ℓ is the activation energy for crack growth, m is a power often found nearly equal to the creep stress exponent n , and B_o is a constant. Equation (4) has had considerable experimental verification and some theoretical justification [3].

2.1.1 Irradiation Effects

Thus far, equations (1), (3) and (4) have precisely the same form as those used previously by the authors to treat the behavior of unirradiated type 316 stainless steel tubes. In this section, those modifications necessary for the treatment of neutron irradiated type 316 stainless steel are described.

The phenomenon of irradiation hardening is most likely to be manifested in the low temperature flow behavior. The effect is handled in this analysis through the hardness parameter, ϵ . To this end, it is useful to employ a theory devised by Whapham and Makin [4] to account for increases in the yield strength σ_I caused by irradiation induced changes in microstructure. Their equation has the form

$$\bar{\sigma}_I = \sigma_1 + (\sigma_s - \sigma_1) \left\{ 1 - \exp\left[-B(\phi t - \phi_o t_o)\right] \right\}^{1/2}; \quad \phi t > \phi_o t_o \quad (5)$$

and

$$\bar{\sigma}_I = \sigma_1; \quad \phi t \leq \phi_o t_o,$$

where B is a material parameter, and ϕt is the total fast neutron fluence for neutrons with energies greater than some specified threshold energy. Here, a threshold fluence $\phi_o t_o$, above which irradiation hardening does not occur, has been introduced [5]. Combining eqs. (1) and (5) allows one to calculate the increment in hardness due to irradiation, ϵ_ϕ . Equation (2) allows calculation of the total hardness for any value of plastic strain as measured from the fully annealed state. It is the contention here that the combination of these equations describes the flow behavior of fast neutron irradiated type 316 stainless steel. Ward and Blackburn [6] have recently published values of the tensile properties, at 658K, of type 316 stainless steel, fast-neutron irradiated at almost constant temperature (659-676K) to various levels of fluence. Figure 1 shows their stress-strain data shifted along the strain (hardness) axis in accordance with Eqs. (1), (2) and (5). Also shown by the solid curve is the flow stress given by Eq. (1) using parameters previously reported by the authors [5]. It is seen that after yielding occurs, all of the data for both irradiated and unirradiated material approach the same flow curve. Since this is the case, it should be pointed out that both unirradiated and irradiated material ought to display the same true ultimate strength, as

defined by the onset of plastic instability. An exception should be observed for the most severe cases of fast neutron exposure, where the material yields at a point on the flow curve beyond the point of plastic instability. Here, one would expect the true ultimate strength to be nearly equal to the true yield strength. This situation is discussed later, with regard to the analysis of tube burst failure at low temperature.

The dominant effect of neutron irradiation on the high temperature mechanical behavior of type 316 stainless steel is a severe loss of ductility arising from an apparent weakening of grain boundaries leading to premature intergranular failure. It is generally believed that this weakening is caused by the presence of helium produced as a result of (n,α) type reactions and precipitated as bubbles on grain boundaries. There is experimental evidence [7] which suggests that, to a first approximation, this process does not affect the high temperature flow properties, but only affects the intergranular failure mechanism. In addition, there is evidence [8] which suggests that the presence of grain boundary bubbles can reduce the apparent activation energy for creep rupture without influencing the creep deformation parameters. Finally, it is generally observed that the embrittling effects of neutron irradiation tend to saturate at some fluence level. Based on these observations, a simplified treatment of the effects of neutron irradiation on the high temperature mechanical behavior of this material is presented here. This is accomplished through a modification of Eq. (4). For unirradiated material it is assumed that $m = n$, and $Q_d = Q_c$ in this equation. In the present analysis, it is proposed that the effect of irradiation is to reduce Q_d by a fluence dependent quantity which approaches a saturation value as fluence increases. This effect can be quantified by examining independent data on the creep-rupture behavior of the irradiated material [7]. An analysis of the observed shift in the Dorn rupture parameter due to irradiation yields [9].

$$(Q_c - Q_d)/R = 3.82 \times 10^3 \text{ Kelvins} \left(1 - \exp \frac{-\phi t}{1.5 \times 10^{22}} \right) \quad (6)$$

3. Analysis of Burst Experiments

3.1 Low Temperature Rupture Behavior

The constant pressure load induces a 2:1 (hoop/axial) stress ratio in the cladding tubes. For relatively large values of initial hoop stress, the high rate of deformation results in failure at low temperatures where plastic flow is essentially strain rate independent. Failure is a consequence of the onset of plastic instability.

The modified Voce correlation (eqs. (1), (2) and (5)) is used to describe the temperature-dependent relationship between the equivalent stress $\bar{\sigma}$ and the hardness $\hat{\epsilon}$. These equations are combined with the Prandtl-Reuss equations in a large strain analysis of thin wall tube deformation. Failure is defined through the definition of the onset of plastic instability for this geometry and loading. The results of these calculations for various fluence levels as compared to experimental determinations of the failure temperature are shown by the dashed curves in Figs. 2 and 3 for heating rates of 5.5 and 111 c/s, respectively. It appears that the inclusion of irradiation hardening in the treatment accounts for the data quite well. The experimentally observed increase in the failure temperature can be explained via the irradiation induced increase in the yield strength beyond the point of plastic instability, as discussed in Section 2.1.1.

3.2 High Temperature Rupture Behavior

For relatively small initial hoop stresses, failure occurs at high temperatures where deformation is strongly strain-rate dependent, and the dominant failure mode is intergranular cracking. A structural feature often observed [1] to accompany failure initiation in this regime is a series of multiple intergranular cracks on the internal surface of the tubes as shown in the schematic tube cross-section of Fig. 4. For this geometry, and sufficiently small crack spacing, G , the mode I stress intensity factor of Eq. (4) is given by [2]

$$K_I = \sigma_\theta \sqrt{G/2} \quad (7)$$

where $\sigma_\theta = Pa/h$ is the hoop stress in the uncracked tendon of thickness h in the tube of radius a . Combining Eqs. (4) and (7) with the kinematic equations defining the strains in the uncracked tendon yields

$$-\frac{1}{a} \frac{da}{dt} (ah) = 2^{-n/2} B_0 \exp\left(-\frac{Q_\ell}{RT}\right) G^{n/2} \left(\frac{Pa}{h}\right)^n \quad (8)$$

Further, by combining the creep law (Eq. (3)) with the Prandtl-Reuss equations, the equilibrium equations, and the kinematic equations, one obtains

$$\frac{1}{a} \frac{da}{dt} = C_0 \exp\left(-\frac{Q_c}{RT}\right) \frac{3^{(n+1)/2}}{2^{(n+1)}} \left(\frac{Pa}{h}\right)^n \quad (9)$$

The algebraic details of the derivations of Eqs. (8) and (9) have been presented elsewhere [2] by the authors.

Since the surface cracks shown in Fig. 4 are intergranular in nature, it is reasonable to assume that their spacing G in Eq. (7) is proportional to the grain size and thereby should follow a grain growth law of the form

$$\frac{dG}{dt} = \frac{F_0}{T} \exp\left(-\frac{Q_G}{RT}\right), \quad (10)$$

where $\frac{Q_G}{R} = 82,000$ K is the activation temperature for grain growth, and F_0 is a constant.

In combination with the definition of Q_ℓ (Eq. (6)), Eqs. (8), (9) and (10) may be integrated numerically to give the failure temperature and failure ductility. The quantities $C_0 = 3.66 \text{ MPa}^{-n} \text{ s}^{-1}$, $Q_c/R = 38,533$ K, and $n = 5.35$ have been extracted from independent tensile experiments [2]. Some useful, and valid approximations [9] to these solutions and the results therefrom are presented here. The crack spacing G^* at the failure temperature T^* is given by

$$G^* = G_0 + \frac{F_0}{T} \frac{RT^*}{Q_G} \exp\left(-\frac{Q_G}{RT^*}\right), \quad (11)$$

where G_0 is the initial spacing and T is the heating rate. Equations (8) and (9) can be integrated, approximately, between the initial radius a_0 and the failure radius a_f to give for the failure ductility

$$(a_f - a_0)/a_0 = \frac{2^{n/2}}{\gamma} \frac{3^{(n+1)/2}}{2^{(n+1)}} \frac{1}{G_0^{n/2}} \exp\left[-\frac{(Q_c - Q_\ell)}{RT^*}\right] \quad (12)$$

where $\gamma = B_o/C_o h_o$. The relationship between initial hoop stress, σ_o , and T^* , for the case of small ductility (<2%), can be obtained, approximately, by setting $a = a_o$ in Eq. (8) and integrating from $h = h_o$, initially, to $h = 0$, giving

$$\sigma_o^S = \left[\frac{2^{n/2}}{\gamma(n+1)} \frac{1}{C_o} \frac{1}{C_o^{n/2}} \exp\left(\frac{Q_l}{RT^*}\right) \frac{Q_l T}{RT^{*2}} \right]^{1/n} \quad (13)$$

For the case of large ductility and very little crack growth Eq. (8) gives, essentially, $ah = a_o h_o$, and this, with Eq. (9), yields

$$\sigma_o^L = \left\{ \frac{2^n}{3^{(n+1)/2}} \frac{1}{nC_o} \frac{Q_c T}{RT^{*2}} \exp\left(\frac{Q_c}{RT^*}\right) \left[1 - \left(\frac{a_f}{a_o}\right)^{-2n} \right] \right\}^{1/n} \quad (14)$$

Equations (12), (13), and (14) can now be used for comparison with the results of tube burst experiments. The unknown coefficients γ , and F_o are fixed relative to the measured ductility maxima for the unirradiated material ($Q_l = Q_c$, Eq. (6)) at the two heating rates. Results for ductility calculations are shown in Figs. (5) and (6) for the 5.5 and 111 c/s experiments respectively. Data [1] is shown for unirradiated material and irradiated material, most of which was exposed to a fluence between $\sim 1 \times 10^{22}$ and $4 \times 10^{22} n/cm^2$. By adjusting Q_l according to Eq. (6), Eq. (12) is plotted for various fluence levels. Showing reasonable agreement, the data fall between the curves corresponding to 1×10^{22} and $10 \times 10^{22} n/cm^2$ in both figures. The results from Eqs. (13) and (14) are shown by the solid curves in Figs. (2) and (3). Here it is seen that the decrease in ductility, predicted to accompany an increase in fluence, can account for the observed decrease in failure temperature for irradiated material.

REFERENCES

- [1] HUNTER, C.W., JOHNSON, G.D., and FISH, R.L., "Mechanical Properties During Simulated Overpower Transients of Fast Reactor Cladding Irradiated from 700-1000°F," HEDL-TME 75-28, Hanford Engineering Development Laboratory, Richland, WA (June 1975).
- [2] KRAMER, J. M. and DIMELFI, R. J., "An Analysis of the Rupture Behavior of Fast Reactor Fuel Cladding Subjected to Thermal Transients," in ASME MPC-8, pp. 315-324 (1978).
- [3] DIMELFI, R. J. and NIX, W. D., "The Stress Dependence of the Crack Growth Rate During Creep," International Journal of Fracture, 13, (3), pp. 341-348 (1977).
- [4] WHAPHAM, A.D. and MAKIN, M. J., "The Hardening of Lithium Fluoride by Electron Irradiation," Phil. Mag., 5, pp. 237-250 (1960).
- [5] KRAMER, J. M. and DIMELFI, R. J., in Reactor Development Program Progress Report, ANL-RDP-77, p. 5.17, Argonne National Laboratory, Argonne, IL (Nov. 1978).
- [6] WARD, A. L. and BLACKBURN, L.D., "Ductility and Strength of FFTF/CRBRP Structural Materials Irradiated in Various Spectra," HEDL-TME 78-51, Hanford Engineering Development Laboratory, Richland, WA (August 1978).
- [7] LOVELL, A. J. and BARKER, R. W., "Uniaxial and Biaxial Creep Rupture of Type 316 Stainless Steel After Fast Reactor Irradiation," in ASTM STP 484, pp. 468-483 (1970).
- [8] GOODS, S. H. and NIX, W. D., "The Kinetics of Cavity Growth and Creep Fracture in Silver Containing Implanted Grain Boundary Cavities," Acta Met. 26, pp. 739-752 (1977).
- [9] DIMELFI, R. J. and KRAMER, J. M., to be published in Reactor Development Progress Report, ANL-RDP-80, Argonne National Laboratory, Argonne, IL (Feb. 1979).

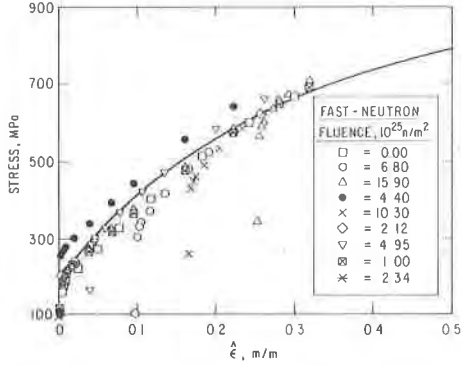


Fig. 1 Flow Stress vs Hardness $\hat{\epsilon}$ (Defined by Eqs. 1 and 2) for Irradiated Annealed Type 316 Stainless Steel for Various Fast-neutron ($E > 0.1$ MeV) Fluences. Voce correlation prediction is given by the curve.

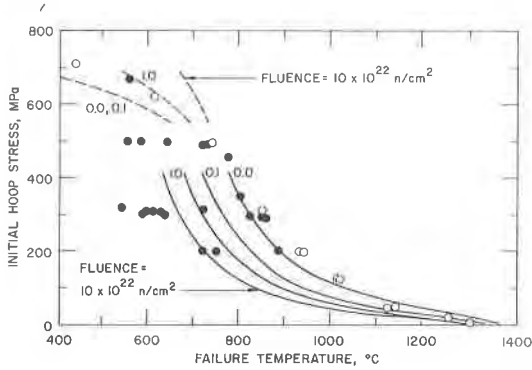


Fig. 2 Failure Temperature for Transient Burst Tests of Unirradiated and Irradiated Fast Reactor Cladding at a Heating Rate of 5.55 c/s. Data for Unirradiated Cladding is given by the Open Symbols. Data for irradiated cladding (fluences of 0.1-4.0 $\times 10^{22}$ n/cm², $E > 0.1$ MeV) is given by the closed symbols. Low-temperature Theoretical results are shown by the dashed curves, while high-temperature theoretical results are shown by the solid curves.

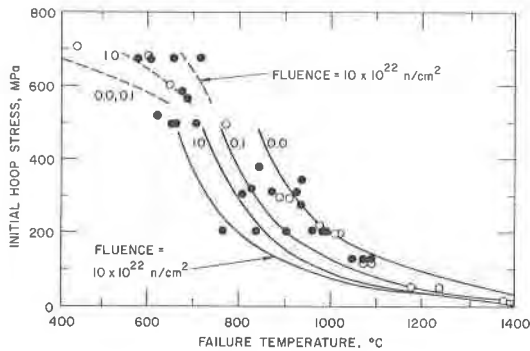


Fig. 3 Same as Fig. 1, except for a heating rate of 111 c/s.

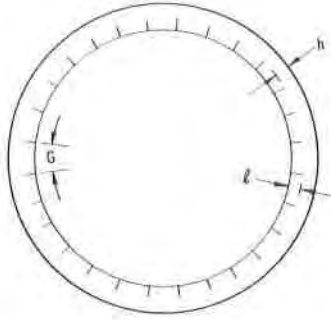


Fig. 4 Crack Geometry

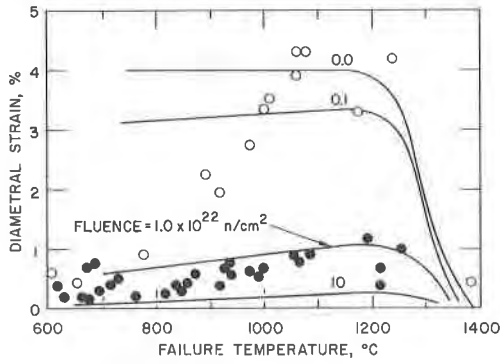


Fig. 5 Diametral Failure Strain for Transient Burst Tests Given in Fig. 2.

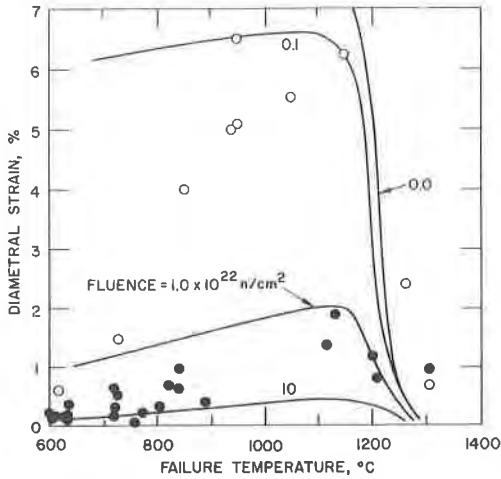


Fig. 6 Diametral Failure Strain for Transient Burst Tests Given in Fig. 3.